Animal Biology, Vol. 56, No. 4, pp. 535-549 (2006)

Also available online - www.brill.nl/ab

Vortex wakes of birds: recent developments using digital particle image velocimetry in a wind tunnel

A. HEDENSTRÖM [1,*], L. VAN GRIETHUIJSEN [2], M. ROSÉN [3], G.R. SPEDDING [4]

[1] *Department of Theoretical Ecology, Lund University, Ecology Building, SE-223 62 Lund, Sweden*
[2] *Experimental Zoology Group, Wageningen University, 6709 PG Wageningen, The Netherlands*
[3] *Department of Animal Ecology, Lund University, Ecology Building, SE-223 62 Lund, Sweden*
[4] *Department of Aerospace and Mechanical Engineering, University of Southern California, Los Angeles, CA 90089-1191, USA*

Abstract—A flying animal generates a trail of wake vortices that contain information about the time history and magnitude of aerodynamic forces developed on the wings and body. Methods for visualising and recording wake vortices have been developed, allowing quantitative measurements by digital particle image velocimetry (DPIV). Results from DPIV experiments in a wind tunnel are presented for four passerine species of differing size and morphology. The normalised vorticity and its integrated quantity, circulation (Γ) both decline gradually with increasing flight speed. The measured circulations are successfully explained by a simple aerodynamic model where a normalised circulation, Γ/Uc, represents half the time-averaged lift coefficient, which is >2 at 4 m s^{-1} for a thrush nightingale.

Keywords: added mass; aerodynamics; bird flight; digital particle image velocimetry; DPIV; vortex wakes.

INTRODUCTION

The vortex wake of a flying animal can be viewed as an aerodynamic 'footprint' containing information about the magnitude and temporal history of aerodynamic forces acting on the animal. In cases where wake structures are organised in geometrically simple forms, the analysis of aerodynamic properties based on vortices is an attractive alternative to the analysis of the motions of the structures (wings or flukes) that generated them. The tight connection between properties of the wake vortices and aerodynamic forces has guided researchers since the 1970s

*Corresponding author; e-mail: hedenstrom@teorekol.lu.se

in their efforts to visualise bird wake structures (Kokshaysky, 1979) and develop aerodynamic models based on wake characteristics (Ellington, 1978; Rayner, 1979a, b, c). Subsequent experimental work focused on quantitative registration of wakes at slow speeds in pigeon *Columba livia* and jackdaw *Corvus monedula* (Spedding et al., 1984; Spedding, 1986), and at a moderate flight speed, $U = 7$ m s^{-1}, of a kestrel *Falco tinnunculus* in flapping and gliding flight (Spedding, 1987a, b). In summary, at slow speed the downstroke develops most aerodynamic force and the wake consists of closed vortex loops, each one the result of the downstroke action, while the upstroke does not generate any significant aerodynamic force, as implied by the absence of significant wake vorticity. At $U = 7$ m s^{-1}, the wake, instead, consists of a pair of trailing vortex tubes following the path of the wing tip. The strength, or circulation, is nearly the same during the down and upstroke, but the distance between the vortices is reduced during the upstroke due to the flexing of the wings. This causes the necessary asymmetry between the two half strokes so that a thrust balances the net drag incurred during the wingbeat cycle. In gliding flight, the wake consists of straight-line vortices that would also be seen behind a fixed winged glider. Quantitatively, the slow speed wake of the pigeon and jackdaw apparently has <50% of the momentum required to support the weight, which was indeed a disconcerting but interesting finding. However, at $U = 7$ m s^{-1}, the vertical momentum flux associated with the trailing vortices matched the weight exactly for both flapping and gliding flight in a kestrel.

The next findings came about following methodological developments in experimental fluid dynamics, and, in particular, the method known as digital particle image velocimetry (DPIV) (Raffel et al., 1997). This method has recently been applied to bird flight in a wind tunnel where vortex wakes of free-flying birds can be recorded under repeatable conditions at different speeds (Spedding et al., 2003b; Rosén et al., 2004; Hedenström et al., 2006). This paper summarises some recent results obtained from our ongoing research on animal flight in the Lund University wind tunnel.

MATERIALS AND METHODS

Bird flight and training

Birds were trained to fly in a low turbulence wind tunnel designed for studies of animal flight (for technical details and baseline flow properties, see Pennycuick et al., 1997). Flow visualisation experiments depend on highly repeatable flight behaviour at the same position in the wind tunnel test section; this was achieved by allowing the bird to sit on a movable perch near the desired flight position. When the perch was lowered, the bird started to fly, and when the bird had flown steadily for a short while (several seconds) in the intended position, the perch was elevated to allow the bird to land and thus get a rest (reward). In this way, we could use a conditioning training procedure that resulted in a highly repeatable, flight behaviour. To guide the bird's orientation in the test section, a visual reference marker was inserted upstream of the flight position. The air speed is the experimental control

Table 1.
Morphological data for bird species used in wind tunnel flow visualisation studies: body mass (m), wing semi-span (b), wing area (S), mean chord (c), aspect ratio (AR) and wing loading (Q = mg/S).

Species	m (g)	b (cm)	S (cm^2)	c (cm)	AR	Q (N/m^2)
Luscinia luscinia	30.5	13.1	126	4.8	5.4	24
Erithacus rubecula	16.5	11.1	104	4.65	4.8	15.6
Phoenicurus phoenicurus	20.1	11.6	111	4.8	4.9	17.8
Delichon urbica	16.9	14.8	112	3.8	7.8	14.8

parameter for most experiments, and most birds would fly at speeds $U = 4$-$11\ \mathrm{m\ s^{-1}}$ or a subset of this range. The species and their morphology studied so far are shown in table 1.

Wing kinematics

Descriptive data about wing beat kinematics are useful when interpreting the wake data. Kinematic measurements usually followed the procedures presented by Rosén et al. (2004), but new digital highspeed video cameras have been obtained which allow three synchronised viewing angles. Frame sequences were usually at a frame rate of 250-500 $\mathrm{s^{-1}}$, shooting from a side view position and a rear view position or, more recently, from one dorsal and two ventral views. The rear view camera was placed approximately 4 m downstream from the bird's position where it causes negligible effects on the airflow in the test section. The position of wing tips, wrists and shoulder joints were digitised from stable flight sequences. From these data the following kinematic properties can be derived: wingbeat period and frequency ($T = 1/f$), down stroke fraction (τ = down stroke duration/T), span ratio (R = (wing span at mid upstroke/wing span at mid down stroke)) and wing tip peak-peak amplitude (A). Kinematic data were collected immediately after a period of flow visualisation because of the different light requirements of DPIV and highspeed video recording. In the current set up, DPIV and high speed video recording are made simultaneously by colour separation, made possible by the fact that DPIV requires dim light conditions and that high speed CCD cameras are infra-red sensitive. Kinematic data are not explicitly presented here but have been used to derive different properties discussed.

Flow visualisation

The DPIV technique used for flow visualisation has been described in great detail elsewhere (Spedding et al., 2003a). In short, the recirculating wind tunnel is filled with thin fog (particle size 1 μm) is illuminated by a double-pulsed laser (Spectra Physics Quanta Ray PIV II, dual head Nd:YAG) emitting green light of wave length 532 nm. A set of mirrors and lenses are used to generate a thin (3 mm) vertical light sheet aligned with the direction of flow (fig. 1). The laser Q-switch (controlling light

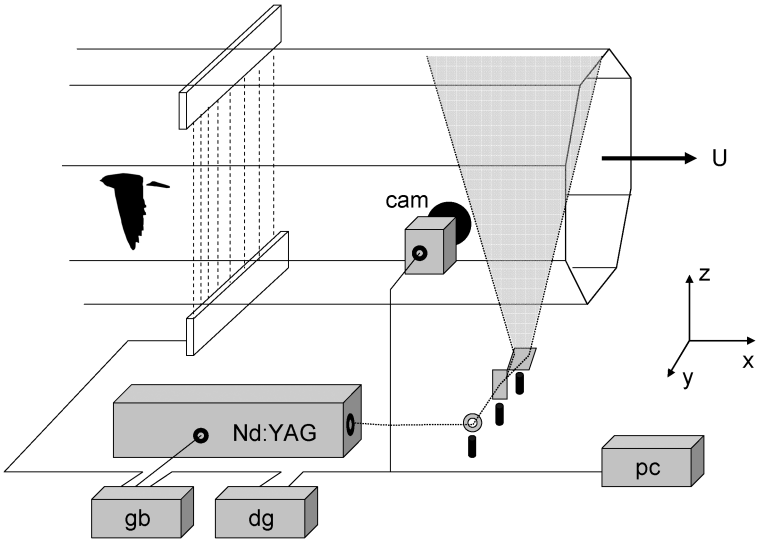

Figure 1. Experimental set up for flow visualisation using Digital Particle Image Velocimetry (DPIV) in a wind tunnel. A bird is flying at speed U in the front half of the test section and the wake disturbance is recorded downstream of the bird by imaging the motion of fog particles between successive pulses of a dual head Nd:YAG laser. The light sheet is generated from the circular beam by a sequence of lenses and directed by two mirrors. The pulses are synchronised with the exposures of a CCD camera (cam), controlled by a delay generator (dg). The bird flies upstream of a curtain of infrared LED-photodiode pairs that, if interrupted, suspend the laser pulses by a gating box (gb). Images are read directly onto a PC hard disk, where they are further processed.

power) and timing of laser pulses (repetition rate 10 Hz) and camera exposures are controlled by a delay generator. The fixed repetition rate of the laser allows the wake to self-sample if the wing beat frequency differs from 10 Hz, which is usually the case. For safety reasons, the bird flies in front of a curtain of infrared LED-photodiode pairs that, if interrupted by the bird, will suspend laser pulses via a gating box (fig. 1). The separation between consecutive exposures δt of an image pair typically varied from 300-800 μs, depending on flight speed and the flow complexity (including the amplitude of cross plane flow components).

Another video camera, positioned in the first diffuser 4 m downstream from the bird, was used to record the bird position in relation to the light sheet. In the rear view the bird is seen in front of the vertical light sheet, allowing classification and grouping of wake images with respect to position along the wing span, left or right wing or if directly downstream from the body.

DPIV analyses

The image pairs obtained from the CCD array camera were analysed using the correlation imaging velocimetry (CIV) technique of Fincham and Spedding (1997). The PIV-delay, δt, was selected to give an average maximum displacement of five pixels between images, when the bandwidth in displacement is 1:100 and the

uncertainty in velocity estimation is approximately ±1% (Spedding et al., 2003a). The mean background free stream flow was removed from the bird wake images to leave the net wake disturbance of the bird only. The velocity components u, v and w are defined in the streamwise (x), spanwise (y) and vertical (z) directions (fig. 1). The images are from the (x, z) plane, and, hence, the calculated vorticity is the spanwise (y) component defined as

$$\omega_y = \frac{\partial w}{\partial x} - \frac{\partial u}{\partial z} \tag{1}$$

where velocity gradients are calculated from analytical differentiation of smoothed spline interpolation coefficients of the velocity field. The uncertainty in the vorticity estimates is approximately ±10% (Spedding et al., 2003a).

By integrating the vorticity over an area S we obtain the circulation, defined as

$$\Gamma = \int_S \omega_y \, \mathrm{d}S \tag{2}$$

which can be considered as a measure of the overall strength of the vortex. In practice, Γ is estimated using a discrete approximation of Equation 2 by the summation of ω_y above a threshold value, typically 20% of maximum in a local neighbourhood, over all contiguous cells. The tails of the distribution are added back by assuming that the sub-threshold vorticity decays as a Gaussian function away from the vorticity peaks. Vorticity and circulations were calculated by this procedure for all large and coherent vortex structures of both signs (sense of rotation), broken down by speed and wing position. Positive circulation is defined as counter clockwise, and for labeling convenience we will refer to those as 'start' vortices, while vortices of the opposing sign are referred to as 'stop' vortices.

It is often convenient to normalise measures of peak vorticity and circulation with respect to flight speed U and wing chord c, as $\Omega = |\omega_y|_{\max} c/U$ and Γ/Uc, respectively. For brevity, the normalised vorticity of positive and negative signed vortices will be denoted Ω^+ and Ω^-, and the associated normalised circulations are denoted Γ^+ and Γ^-, respectively.

A central question is that of possible force balance on the basis of wake momentum, especially at very slow speeds where previous experiments have failed to recover enough momentum flux for weight support (Spedding et al., 1984, Spedding, 1986). If all wake vorticity is the result of the downstroke and confined to discrete loops with an inactive upstroke, then the circulation required to support the weight W is

$$\Gamma_1 = \frac{WT}{\rho S_e} \tag{3}$$

where T is the wingbeat period, ρ is air density and S_e is the horizontally-projected area of the vortex loop (Spedding, 2003b; Hedenström et al., 2006). This quantity is used as a rough measure of whether the wake circulation is close to that required.

RESULTS

Wake topology

The overall 3D topology can be deduced from 2D wake images along different stations of the wingspan. Examples of typical composite wake images are shown for the redstart at $U = 5$ m s^{-1}, a relatively slow or intermediate speed, and at $U = 8$ m s^{-1}, a normal cruising speed for a small passerine. The slow speed wake is dominated by isolated vortex patches with a comparatively concentrated and well-defined start vortex, being the result of the start of the downstroke when lift is increased on the wing and the concomitant shedding of a start vortex (fig. 2a). The stop vortex is also evident at the transition between the down and upstroke, but it is less well defined and its peak vorticity magnitude is significantly less than the corresponding start vortex. This pattern and asymmetry between start and stop vortices is found in all species investigated (fig. 2a; Spedding et al., 2003b; Hedenström et al., 2006; M. Rosén, G.R. Spedding, A. Hedenström, unpubl. data).

Even at speeds as low as 4-5 m s^{-1} there is typically some vorticity shed throughout the upstroke, suggesting that some aerodynamic force is generated. When the speed increases, the vorticity shed becomes more uniform throughout the wingbeat, with peak start and stop structures converging to the same circulation (fig. 2a). This is consistent with the notion of a wake of constant circulation and hence the same span-specific lift force throughout the wing beat. The upstroke takes on an increasing role as lift-producing function, but the reduced span during the upstroke maintains the asymmetry between down- and upstroke to achieve positive thrust. Cartoon interpretations of the wake for the redstart at $U = 5$ and 8 m s^{-1} are shown in figure 2b. The cruising speed wake is not the idealised wake of undulating trailing vortices (Spedding, 1987a), but there seems to be a continuous shedding of span-wise vorticity (fig. 2a, and similar composites in Spedding et al., 2003b; Rosén et al., 2004; Hedenström et al., 2006).

Wake vorticity and circulation

Quantitatively, the vorticity Ω associated with the primary start and stop vortices declines from slow to high speeds and Ω^+ is higher than Ω^- for slow speeds but, with increasing U, the values converge and at $U \geqslant 6$ m s^{-1} they are indistinguishable (fig. 3; Spedding et al., 2003b; Hedenström et al., 2006). This pattern also holds for Γ^+ and Γ^- with declining values with increasing flight speed (fig. 3). The pattern shown in figure 3 for the house martin is general for all investigated species so far, but the absolute values of Ω and Γ differ among species. In order to understand which factors determine the measured Γ, consider the Kutta-Juokowski lift on a wing of finite span $2b$

$$\Gamma = \frac{W}{\rho 2bU} = \frac{Wc}{\rho SU} \tag{4}$$

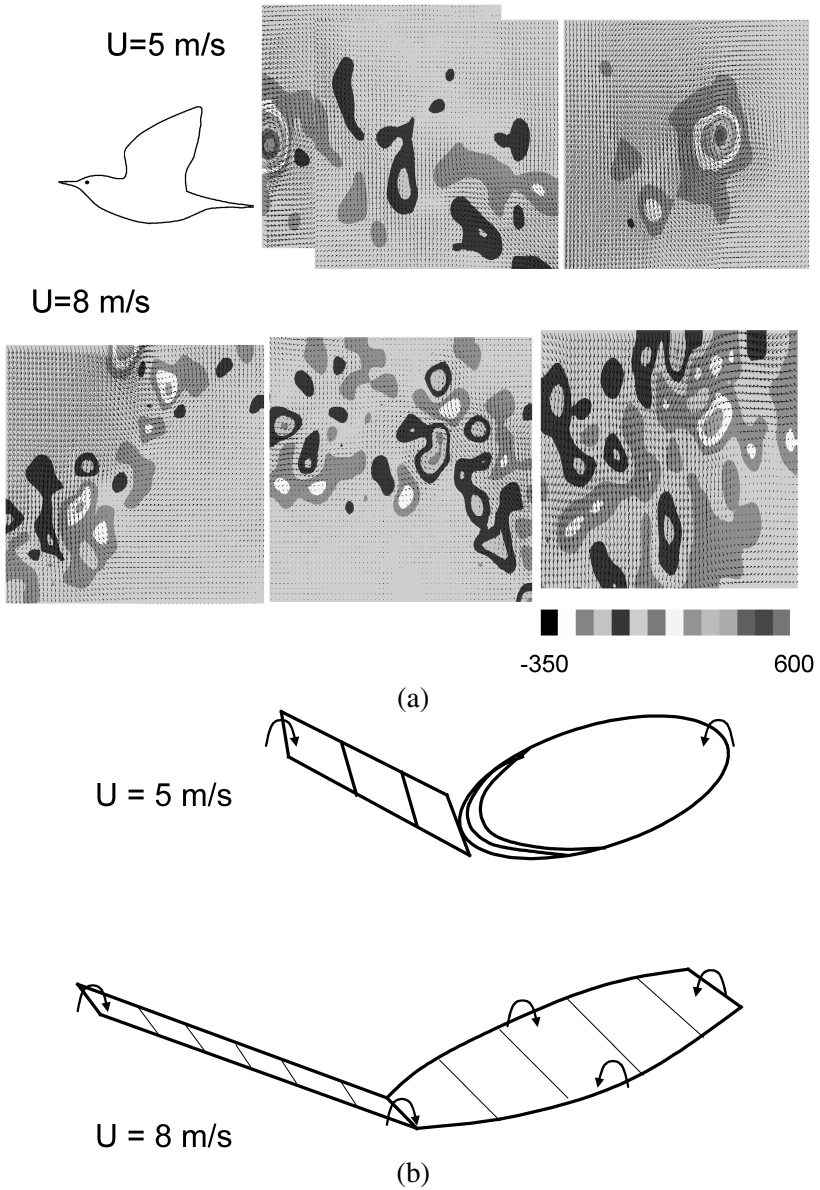

Figure 2. (a) Composite of wake pattern at $U = 5$ and 8 m s^{-1} for a redstart. Data are from the vertical centreplane. The vorticity is mapped asymmetrically about a 14-step colour bar to local extrema of -350 and 600 s^{-1}. At 5 m s^{-1} the start vortex is relatively strong and well defined, but not all positive vorticity is confined to the main structure, shown by the traces of vorticity throughout the wingbeat. At 8 m s^{-1} the vorticity appears more continuously throughout the wing beat, and the main vortex patches are less dominant. The images are from a plane directly downstream from the body of the bird. Flight direction is from right to left as indicated by the bird silhouette. (b) Cartoon summary of the wake pattern deduced from vortex wake images as shown in (a). The two wake types do not represent discrete vortex topologies since the transition from one to another is gradual when speed is changed. Arrows indicate sense of circulation.

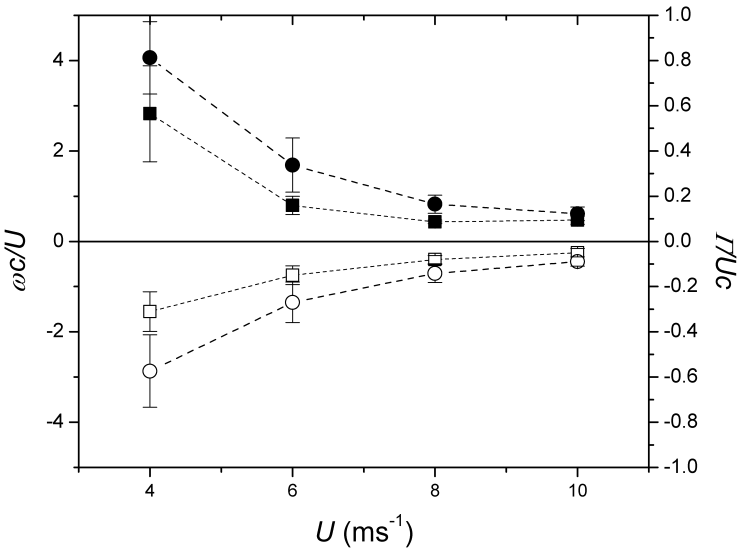

Figure 3. Variation with flight speed in peak vorticity magnitude $|\omega|_{\max} c/U$ (squares) and measured circulation Γ/Uc (circles) of the strongest starting (filled symbols) and stopping (open symbols) vortices for a house martin. Symbols represent mean ±1SD. Vorticity values are indicated on the left vertical axis and circulation on the right vertical axis, respectively.

where ρ is the air density, S is the wing area, c is the mean chord, U is the airspeed and W is the weight. This equation expresses the theoretically-predicted circulation that would be measured for a steady flying-wing at constant speed U. Plotting Equation 4 with the measured circulation and body geometry of the redstart and house martin shows that agreement between theory and data is reasonably good (fig. 4). An extended data set including previously published data adds support to this conclusion (Hedenström et al., 2006). Data from a kestrel flying at $U = 7$ m s^{-1} (Spedding, 1987b) measured using another PIV-technique based on stereo-photogrammetric tracing of individual helium filled soap bubbles, and where force balance was found on measured circulation, also fit nicely into this simple theoretical framework (Hedenström et al., 2006), as do circulations measured for a pigeon and jackdaw flying at slow forward flight speed (Hedenström et al., 2006).

Taking it one step further, the quantities of ordinate and abscissa of figure 4 could be normalised as Γ/Uc and U/U_{mp}, where U_{mp} is the minimum power speed (Pennycuick 1989; v 1.16). At U_{mp}, the power required to fly is minimised, but for our purpose it is only used as a benchmark to standardise speed among species, and the assumptions concerning various model parameters, such as the controversial body drag coefficient $C_{\mathrm{D,par}}$ (Hedenström, 2002), are of no importance. Figure 5 shows the accumulated data for five individuals of four species (table 1), where all data points appear to converge onto the same curve. By dividing both sides Equation 4 with Uc we obtain

$$\frac{\Gamma}{Uc} = \frac{W}{\rho S U^2} = \frac{W}{2qS} \tag{5}$$

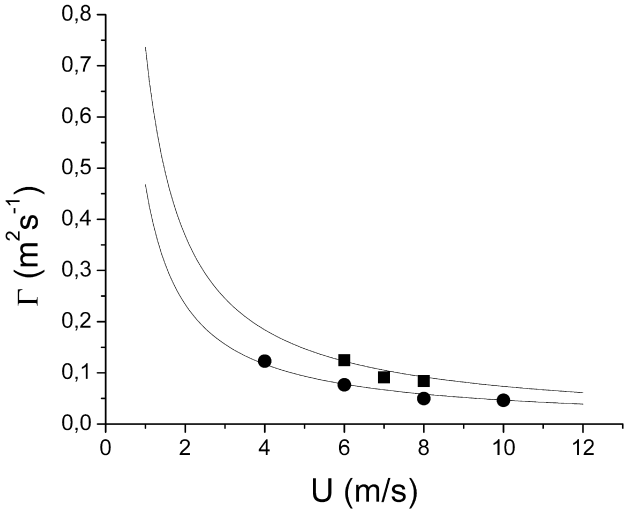

Figure 4. Predicted (continuous lines) and measured circulation (symbols) for a redstart (upper curve, squares) and a house martin (lower curve, circles). The lines are calculated using Equation 4 as derived from Hedenström et al. (2006). The house martin data are from Rosén, Spedding and Hedenström, (unpubl. data).

where $q = \frac{1}{2}\rho U^2$ is the dynamic pressure. The left hand side is the quantity plotted on the ordinate of figure 5. The lift on a wing of planform area S can be expressed as

$$L = qSC_L \tag{6}$$

where C_L is a dimensionless lift coefficient. Since $L = W$ at steady level flight, rearranging Equation 6 to solve for C_L yields the same expression as the right hand side of Equation 5, i.e., Equation 5 represents a lift coefficient, as noted in Rosén et al. (2006). The fact that experiment and theoretical curves agree closely in figure 5 suggests that these birds fly at approximately similar lift coefficients. Combining Equations 5 and 6 shows that $\Gamma/Uc = C_L/2$. Since $\Gamma/Uc \simeq 1.2$ at $U = 4$ m s^{-1} the time-averaged $C_L > 2$.

Force balance

At slow speeds (4-5 m s^{-1}) the circulation confined to the main start/stop vortex structure was approximately 50% of the reference circulation Γ_1 required for weight support for both the thrush nightingale and robin (Spedding et al., 2003b; Hedenström, et al., 2006), apparently repeating the previous results suggesting a wake momentum deficit. This, however, assumes that all same-signed vorticity is confined to a single vortex structure. Inspection of the wake images suggested that the true vorticity distribution deviated from the idealised loops assumed in Equation 3, and that patches of positive vorticity occurred also at the transition between down/upstroke, otherwise dominated by negative vorticity. Some positive vorticity

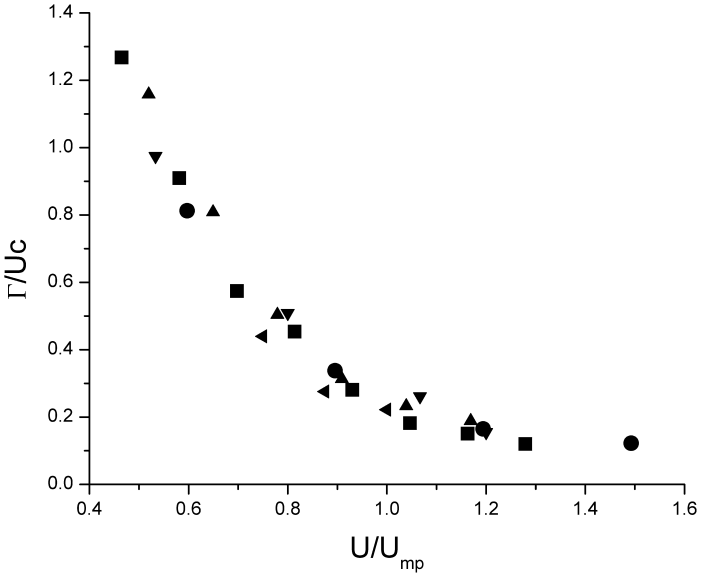

Figure 5. Normalised circulation (Γ/Uc) in relation to flight speed relative to calculated minimum power speed U_{mp} for the species in table 1. The symbols represent thrush nightingale (■), house martin (●), robin #1 (▲), robin #2 (▼), and redstart (◄).

was also associated with the upstroke. Adding all same signed vorticity from the whole wingbeat, including the low amplitude patches outside the dominating vortex patches, resulted in measured circulations near Γ_1; measurements were, therefore, consistent with weight support (Spedding et al., 2003b; Hedenström et al., 2006). Also in the house martin it was necessary to add the same-signed vorticity to that from the region around the transition between down-/upstroke in order to get $\Gamma_{obs}/\Gamma_1 \approx 1$ (M. Rosén, G.R. Spedding, A. Hedenström, unpubl. data). These findings show that while the wake possesses the required circulation, its distribution deviated significantly from the vortex loop model at slow speed. Note that only the vertical force component was considered, which is justified for the purpose of a crude check of force balance since L is typically one order of magnitude higher than D. In reality, though, the wake impulse must balance the resultant aerodynamic force which also includes the drag, or resistance to forward motion (see below).

DISCUSSION

The successful application of DPIV methods to free-flying birds has already resulted in a number of new insights about the aerodynamics of flapping flight. The vorticity and circulation vary smoothly over the speed range without any obvious discontinuities, suggesting that the wake is transformed from loop-type structures at slow speeds, with increasing vorticity shedding during the upstroke at intermediate speeds and, eventually, a more or less uniform vortex shedding throughout the wing

stroke. This notion is supported from analyses of changes in wingbeat kinematics, which also show gradual changes over the speed range (Rosén et al., 2004). In the thrush nightingale and robin, the span ratio, defined as the ratio between wing span at mid-upstroke to that at mid-downstroke, increased somewhat with increasing speed (Rosén et al., 2004; Hedenström et al., 2006), which was interpreted as a sign of increased aerodynamic significance. However, the opposite trend was found for a house martin and the similar barn swallow (Park et al., 2001). The reason for this difference is not entirely clear, but could be due to the different wing morphology between the martin/swallow and the turdines (table 1), affecting the general flight style.

Dabiri (2005) has noted that vortex wake signatures can be accompanied by a 'vortex added-mass', where fluid surrounding vortex structures is accelerated into motion in a potential flow. A full accounting for a wake momentum flux will, therefore, require estimates of both vortical motions and non-vortical added-mass components. Since the latter do not appear in circulation measures derived from vorticity fields, there is a possibility that a significant fraction of the momentum flux is omitted. A dimensionless 'wake vortex ratio' of the relative importance of vortex and added-mass forces was suggested as

$$Wa = \frac{c_a l_v U_v}{\Gamma}$$

where c_a is a wake-vortex added mass coefficient of a vortex structure of length l_v (in the direction of propagation) at self-induced convection velocity U_v and circulation Γ. A characteristic value for *Wa* can be estimated for practical DPIV-based bird wake experiments such as reported here, using the thrush nightingale data of Spedding et al. (2003b) as an example. Significant added mass effects will be more likely at lower flight speeds, when accelerations of both the body and the surrounding fluid are strongest. At $U = 4$ m/s, the average measured circulation of the start vortex was $\Gamma = 0.25$ m^2 s^{-1}. A typical structure length can be estimated as $l_v = 0.04$ m (figs 9, 10; Spedding, 2003b), and a mean convection velocity can be estimated either from the estimated motion of the structure from the position of the bird to its point of measurement (both are known) or from the theoretical convection velocity of a circular vortex ring of similar size and strength (Lamb, 1932). Both estimates give $U_v = 0.5$ m s^{-1}. Using $c_a = 0.72$, as estimated for a piston-generated vortex ring in Dabiri (2005), $Wa = 0.06$ for the thrush nightingale at its slowest flight speed. Dabiri suggested a criterion for significance of added mass effects by comparing *Wa* with the magnitude of the experimental uncertainty in measurements of Γ, but this confuses the measurement of the physical phenomenon with its dynamical significance which is better evaluated from *Wa* itself. In a follow-up study, Dabiri et al. (2006) suggest that added mass effects should be considered if $Wa > c_a/(1 + c_a)$, which evaluates to 0.42 , seven times greater than estimated for the thrush nightingale in slow-speed flight. As measured by this criterion, vortex added-mass terms are unimportant for any bird flight experiments conducted thus far.

The practical difficulties in estimating even time-averaged forces from assemblages of thousands of independent, two-dimensional slices through a complex three-dimensional wake should not be understated, and certain, quite strong, assumptions underlie the approximate momentum-balance checks noted thus far. In particular, the method of adding up all same-signed vorticity (i.e., to Γ_{tot}) and calculating the vertical impulse as if there had been a simple elliptical loop whose constant circulation is equal to Γ_{tot} is a significant simplification. The result cannot claim to be anything more than a rough check, and differences of $\pm 20\%$ are not considered important at this level of approximation. The feasibility of making momentum-balance calculations at all in complex and possibly turbulent wakes has been questioned by Tytell and Ellington (2003) who reported the shortfall in calculated momentum of initially laminar, piston-generated vortex rings as they destabilised and became turbulent. The onset of turbulence was noted for dimensionless times

$$t^* = \frac{\nu t}{16 R_{\text{r}}^2} \tag{7}$$

where t is the elapsed time in seconds and R_{r} is the ring radius. For an initial ring Reynolds number, $Re_{\text{r}} = \Gamma/\nu = 4.5 \times 10^3$, turbulent decay that reduced the calculated ring momentum was reported at ca. $t^* = 7 \times 10^{-4}$. In earlier pigeon and jackdaw studies (Spedding et al., 1984; Spedding, 1986), which are the only such studies reporting an apparent momentum deficit, the wakes were measured almost immediately after their formation, so $t \approx 1/f$, and approximating $R \approx b$ (the wing semispan), t^* can be estimated from the original data and from a summary in Hedenström et al. (2006) as 1.3×10^{-6} for the pigeon and 1.9×10^{-6} for the jackdaw. While Re_{r} for the bird wakes is indeed larger (ca. 20 times) than for the experiments of Tytell and Ellington, t^* is more than 300 times less than required for significant turbulent diffusion or dissipation. Moreover, as noted previously, Spedding et al. (2003b) found that an apparent momentum deficit of around 50% would be expected, given the inability of the previous measurement methods to measure accurately small and complex distributions of vorticity. The improved measurement technique showed that there is no deficit. Even in older experiments no momentum deficit was found from wake measurements of a kestrel in either gliding or flapping flight, hence the conclusion that force balance measurements cannot be made in moderate *Re* wakes is clearly false and rather illustrates the difficulty in comparing wakes of flapping animal wings with those generated by pistons. The important concept is that of making appropriate approximations, both in experiment and in theoretical models (or, very often, combinations of the two). The simplifications used in the bird wake analysis are indeed strong, and so limit the conclusions to approximate ones that are only as good as the model used to make further inferences – on the adequacy of the wake impulse for wake support, for example. The same applies to mechanical analogues.

As a footnote, it is notable that the wakes measured far from their point of origin (see below) are not more complex than they are. The marginal stability of flows over

airfoils at moderate *Re* is well known, and the complexity (or lack thereof) of the far wake can be argued to imply a rather fine control of the local flow over the flapping, feathered surface such that a coherent, repeatable signature can still be distinguished further downstream. An appropriate physical model analogue, at the same *Re*, for a simple feathered (and possibly flapping) wing system, has never been constructed and is a topic of current research.

Spedding et al. (2003b) noted that the net horizontal force in the wake of a self-propelled body in unaccelerated motion will be precisely zero. However, if the viscous drag wakes can be separated topologically from the primary propulsive vortex system in the same wake, then it might still be possible to estimate net drag forces. The drag wake can easily be identified during brief glides of the thrush nightingale when they are not obscured by the more complicated flapping flight wake. Hence, a complete and accurate force-balance based on glide wakes looks more promising than for flapping flight. As noted above, complications in measurement and analysis arise because, for practical reasons, the bird wakes are currently imaged some distance ($\sim 18c$) downstream from the point of generation, and during the time since shedding from the wings the wake has distorted and evolved in not uncomplicated ways. A comparison of the measured momentum defect in wakes at $2c$ and at $12c$ downstream of a fixed wing showed no loss of measured momentum at all measured angles of attack, despite the notable increase in wake irregularity (Spedding et al., 2006). Although this shows that momentum conserving wake measurements can be made far downstream, it is still much more difficult to know how to construct appropriate control volumes when the wake structure is complicated, and there would be much interest in measuring bird wakes closer to their source.

The DPIV technique has demonstrated several intriguing facts about bird flight kinematics and aerodynamics. It has also recently been used to investigate the asymmetry between down and upstroke in hovering hummingbirds (Warrick et al., 2005). Further developments will include the systematic investigation of gliding flight using the tiltable wind tunnel, because here the $L{:}D$ ratio is given by the glide ratio as an independent check. Investigation of bounding/intermittent flight also remains to be done. Improvements would also accrue from the use of lasers of higher repetition rate allowing an improved time resolution of wake dynamics, and the use of 3D DPIV for instantaneous three-dimensional spatial characterisation of wake flow. The latter will help to distinguish between vortex wakes due to inviscid force generation and viscous drag, and hence improve the prospect of estimating the total aerodynamic forces based on aerodynamic 'footprints' only.

ACKNOWLEDGEMENTS

The research was supported by the Knut and Alice Wallenberg foundation, the Carl Tryggers foundation, the Swedish Research Council and the Swedish Foundation for International Cooperation in Research and Higher Education (STINT) (to

A. Hedenström). A. Hedenström is a Royal Swedish Academy of Sciences Research Fellow supported by a grant from the Knut and Alice Wallenberg Foundation. This study was approved by the Lund University Ethical committee for the use of live animals in research and follows the legal requirements in Sweden for keeping animals in captivity for research purposes.

REFERENCES

Dabiri, J.O. (2005) On the estimation of swimming and flying forces from wake measurements. *J. Exp. Biol.*, 208, 3519-3532.

Dabiri, J.O., Colin, S.P. & Costello, J.H. (2006) Fast-swimming jellyfish exploit velar kinematics to form an optimal vortex wake. *J. Exp. Biol.*, 209, 2025-2033.

Fincham, A. & Spedding, G.R. (1997) Low-cost, high resolution DPIV for measurement of turbulent fluid flow. *Exp. Fluids*, 23, 449-462.

Hedenström, A. (2002) Aerodynamics, evolution and ecology of bird flight. *Trends Ecol. Evol.*, 17, 415-422.

Hedenström, A., Rosén, M. & Spedding, G.R. (2006) Vortex wakes generated by robins *Erithacus rubecula* during free flight in a wind tunnel. *J. R. Soc. Interface*, 3, 263-276.

Kokshaysky, N.V. (1979) Tracing the wake of a flying bird. *Nature*, 279, 146-148.

Pennyuick, C.J. (1989) *Bird Flight Performance: A Practical Calculation Manual*. Oxford University Press, Oxford.

Pennyuick, C.J., Alerstam, T. & Hedenström, A. (1997) A new low-turbulence wind tunnel for bird flight experiments at Lund University, Sweden. *J. Exp. Biol.*, 200, 1441-1449.

Raffel, M., Willert, C.E. & Kompenhans, J. (1997) *Particle Image Velocimetry: A Practical Guide*. Springer, Berlin.

Rayner, J.M.V. (1979a) A vortex theory of animal flight. I. The vortex wake of a hovering animal. *J. Fluid Mech.*, 91, 697-730.

Rayner, J.M.V. (1979b) A vortex theory of animal flight. II. The forward flight of birds. *J. Fluid Mech.*, 91, 731-763.

Rayner, J.M.V. (1979c) A new approach to animal flight mechanics. *J. Exp. Biol.*, 80, 17-54.

Rosén, M., Spedding, G.R. & Hedenström, A. (2004) The relationship between wingbeat kinematics and vortex wake of a thrush nightingale. *J. Exp. Biol.*, 207, 4255-4268.

Spedding, G.R. (1986) The wake of a jackdaw (*Corvus monedula*) in slow flight. *J. Exp. Biol.*, 125, 287-307.

Spedding, G.R. (1987a) The wake of a kestrel (*Falco tinnunculus*) in gliding flight. *J. Exp. Biol.*, 127, 45-57.

Spedding, G.R. (1987b) The wake of a kestrel (*Falco tinnunculus*) in flapping flight. *J. Exp. Biol.*, 127, 59-78.

Spedding, G.R., Rayner, J.M.V. & Pennyuick, C.J. (1984) Momentum and energy in the wake of a pigeon (*Columba livia*) in slow flight. *J. Exp. Biol.*, 111, 81-102.

Spedding, G.R., Rosén, M. & Hedenström, A. (2003a) Quantitative studies of the wakes of freely-flying birds in a low turbulence wind tunnel. *Exp. Fluids*, 34, 291-303.

Spedding, G.R., Rosén, M. & Hedenström, A. (2003b) A family of vortex wakes generated by a thrush nightingale in free flight in a wind tunnel over its entire natural range of flight speeds. *J. Exp. Biol.*, 206, 2313-2344.

Spedding, G.R., McArthur, J. & Rosén, M. (2006) Deducing aerodynamic mechanisms from near- and far-wake measurements of fixed and flapping wings at moderate Reynolds number. *AIAA J.*, (in press).

Tytell, E.D. & Ellington, C.P. (2003) How to perform measurements in a hovering animal's wake: physical modeling of the vortex wake of the hawkmoth, *Manduca sexta*. *Phil. Trans. R. Soc. Lond. B*, 358, 1559-1566.

Warrick, D.R., Tobalske, B.W. & Powers, D.P. (2005) Aerodynamics of the hovering hummingbird. *Nature*, 435, 1094-1097.